ACS NANO
Cite This: ACS Nano 2019, 13, 14145−14151
www.acsnano.org
ARTICLE

Downloaded via UNIV OF MASSACHUSETTS AMHERST on December 31, 2019 at 15:14:06 (UTC).
See https://pubs.acs.org/sharingguidelines for options on how to legitimately share published articles.

Highly Transparent Contacts to the 1D Hole Gas in Ultrascaled Ge/Si Core/Shell Nanowires

Masiar Sistani,[†,¶] Jovian Delaforce,[‡,¶] Roman B. G. Kramer,[‡] Nicolas Roch,[‡] Minh Anh Luong,[§] Martien I. den Hertog,[‡] Eric Robin,[§] Jürgen Smoliner,[†] Jun Yao,[∥] Charles M. Lieber,[⊥,#] Cecile Naud,[‡] Alois Lugstein,[†] and Olivier Buisson*[,‡]

[†]Institute of Solid State Electronics, TU Wien, Gußhausstraße 25-25a, 1040 Vienna, Austria
[‡]Université Grenoble Alpes, CNRS, Institut NEEL UPR2940, F-38054 Grenoble, France
[§]Université Grenoble Alpes, CEA, IRIG-DEPHY, F-38054 Grenoble, France
[∥]Department of Electrical and Computer Engineering, Institute for Applied Life Sciences, University of Massachusetts, Amherst, Massachusetts 01003, United States
[⊥]Department of Chemistry and Chemical Biology, Harvard University, Cambridge, Massachusetts 02138, United States
[#]School of Engineering and Applied Science, Harvard University, Cambridge, Massachusetts 02138, United States

S *Supporting Information*

ABSTRACT: **Semiconductor−superconductor hybrid systems have outstanding potential for emerging high-performance nanoelectronics and quantum devices. However, critical to their successful application is the fabrication of high-quality and reproducible semiconductor−superconductor interfaces. Here, we realize and measure axial Al−Ge−Al nanowire heterostructures with atomically precise interfaces, enwrapped by an ultrathin epitaxial Si layer further denoted as Al−Ge/Si−Al nanowire heterostructures. The heterostructures were synthesized by a thermally induced exchange reaction of single-crystalline Ge/Si core/shell nanowires and lithographically defined Al contact pads. Applying this heterostructure formation scheme enables self-aligned quasi one-dimensional crystalline Al leads contacting ultrascaled Ge/Si segments with contact transparencies greater than 96%. Integration into back-gated field-effect devices and continuous scaling beyond lithographic limitations allows us to exploit the full potential of the highly transparent contacts to the 1D hole gas at the Ge−Si interface. This leads to the observation of ballistic transport as well as quantum confinement effects up to temperatures of 150 K. Low-temperature measurements reveal proximity-induced superconductivity in the Ge/Si core/shell nanowires. The realization of a Josephson field-effect transistor allows us to study the subgap structure caused by multiple Andreev reflections. Most importantly, the absence of a quantum dot regime indicates a hard superconducting gap originating from the highly transparent contacts to the 1D hole gas, which is potentially interesting for the study of Majorana zero modes. Moreover, underlining the importance of the proposed thermally induced Al−Ge/Si−Al heterostructure formation technique, our system could contribute to the development of key components of quantum computing such as gatemon or transmon qubits.**

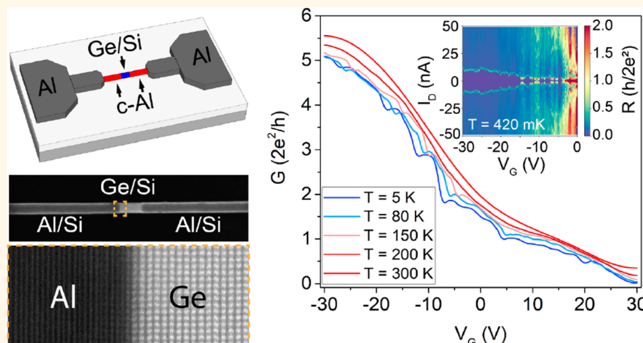

KEYWORDS: *nanowire heterostructure, germanium, 1D hole gas, superconductor−semiconductor hybrids, hard superconducting gap, transparent contacts*

The capability to customize the morphology and size of low-dimensional nanostructures, such as nanowires (NWs), and thus tune the associated electronic and optical properties, has triggered substantial research interest.[1−4] Especially, band-structure engineering by controlled epitaxial growth of core/shell NWs has provoked the investigation of 1D hole-gas systems,[4] attractive for fundamental studies of low-dimensional transport as well as future high-performance nanoelectronic or quantum devices.[5−9] Further, heterostructures of dissimilar materials with structure−property relationships and interactions originating from the contributions of individual low-dimensional components

Received: August 27, 2019
Accepted: December 9, 2019
Published: December 9, 2019

ACS Publications © 2019 American Chemical Society

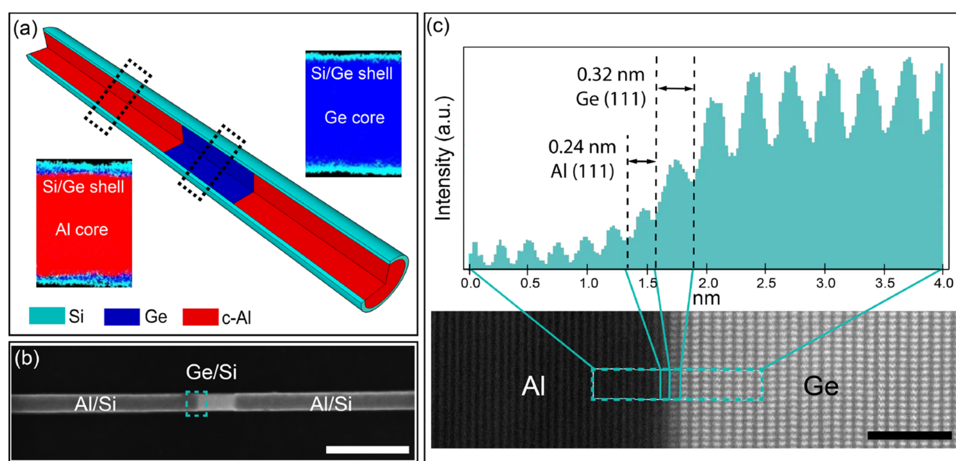

Figure 1. (a) Schematic illustration of an axial Al−Ge−Al NW heterostructure with an ultrathin semiconducting shell wrapped around it. The insets show EDX chemical maps at the respective positions along the heterostructure indicating an intact semiconducting shell around the entire Al−Ge−Al heterostructure. (b) SEM image of the actual heterostructure arrangement. Scale bar is 200 nm. (c) High-resolution HAADF STEM obtained at the Al−Ge interface and corresponding intensity profile obtained at the cyan dashed square shown in (b). Scale bar is 2 nm.

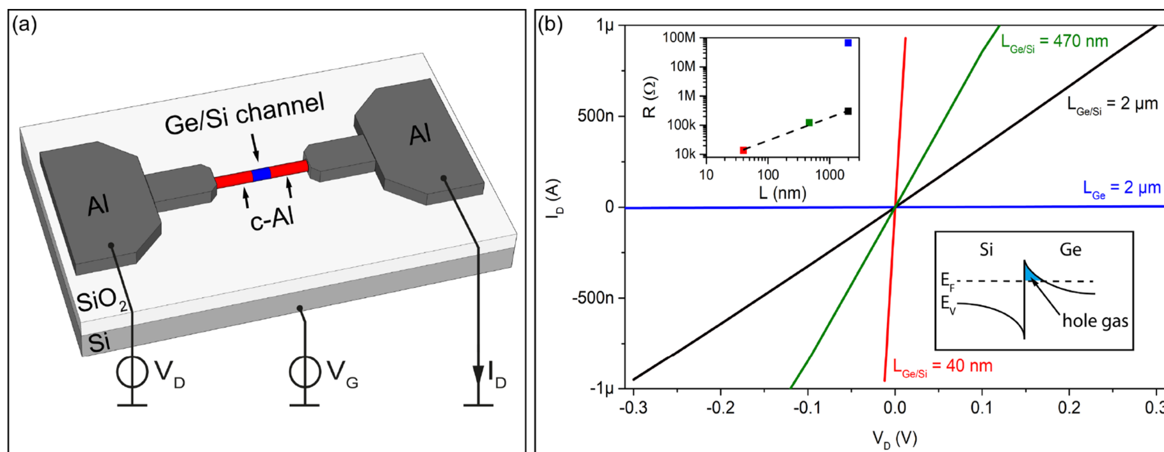

Figure 2. (a) Schematic illustration of the heterostructure NWs integrated in a back-gated FET configuration. (b) Comparison of the *I*/*V* characteristic of an intrinsic Ge NW (blue), a Ge/Si core/shell NW (black), and Al−Ge/Si−Al heterostructure device with varying channel lengths of $L_{Ge/Si}$ = 470 nm (green) and $L_{Ge/Si}$ = 40 nm (red) achieved by consecutive annealing steps. The upper inset shows the resistance of the respective devices *versus* the channel length. A band diagram at the Ge/Si heterojunction in Ge/Si core/shell NWs is shown in the lower inset. E_V and E_F are the valence band edge and the Fermi energy, respectively.

may enable electronic or photonic devices that are outclassing or even unattainable for planar geometries.[10,11] However, fabricating interconnects is a crucial step toward the integration of such future ultrascaled devices and requires sophisticated nanostructure formation techniques and precise lithography. To overcome these limitations, material combinations with no intermetallic phase formation, such as the Al−Ge system, enabling true metal−semiconductor heterostructures with abrupt metal−semiconductor interfaces received a considerable amount of attention.[12−17] Within this paper, we apply quasi 1D superconducting Al leads to ultrascaled Ge/Si core/shell channels forming highly transparent contacts to the 1D hole gas. Such a monolithic superconductor−semiconductor heterostructure enables an exchange of Cooper pairs between two highly transparent superconducting contacts through the hole gas. This leads to supercurrent induced by the superconducting proximity effect,[18] which is an important prerequisite for a Josephson field-effect transistor (JoFET), which could be integrated into a gate-tunable superconducting qubit, often referred to as a gatemon.[19] Further, this architecture due to the strong spin−orbit coupling of holes in Ge could be an attractive candidate for the study of Majorana zero modes and development of topological superconducting qubits.[16,20]

RESULTS AND DISCUSSION

Our approach for the synthesis of a monolithic Al−Ge/Si−Al NW heterostructure featuring highly transparent contacts to a 1D hole gas is based on vapor−liquid−solid[21] grown core/shell NWs with a Ge NW core diameter of 30 nm and a Si-shell thickness of about 3 nm. For such NWs contacted by Al pads we demonstrate the realization of tunable Ge segment lengths by the substitution of the Ge core by crystalline Al (c-Al) utilizing a thermally induced exchange reaction while maintaining the ultrathin semiconducting shell wrapped around it (Figure 1a).[13] We note that in this exchange reaction all Ge atoms of the original NW are replaced by Al atoms, with the exception of a thin surface layer (2 nm or less)

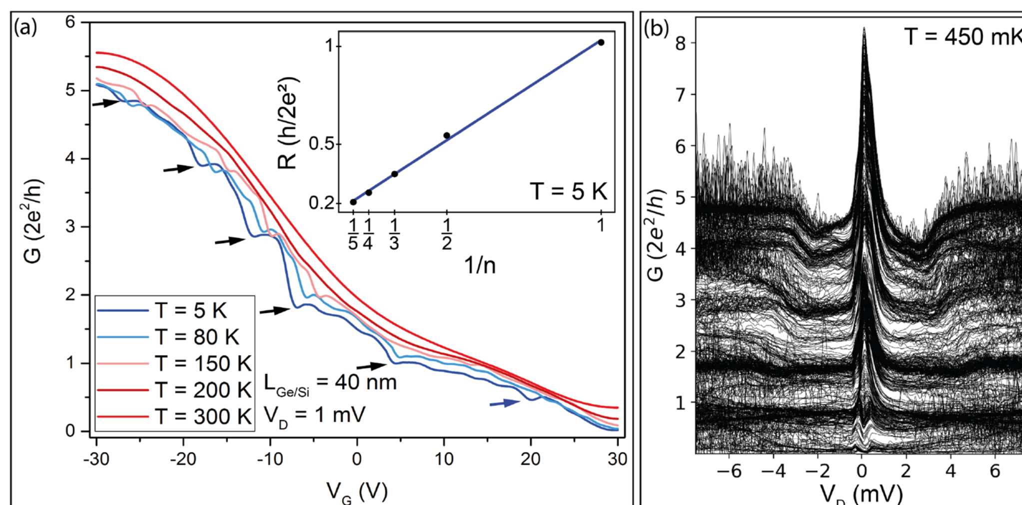

Figure 3. (a) $G-V_G$ characteristics of the Al−Ge/Si−Al heterostructure device with a channel length of $L_{Ge/Si}$ = 40 nm measured at different temperatures between T = 5 and 300 K. The conductance G was directly obtained from the measured current as the V_G is swept from −30 to 30 V according to $G = I_D/V_D$ and is plotted in units of G_0. The black arrows indicate the quantized conductance plateaus, and the blue arrow indicates the $0.7G_0$ plateau at 5 K. The inset shows the resistance (R) of the quantized conductance plateaus *vs* the inverse of the conducting channel number ($1/n$). (b) $G = I_D/V_D$ with series resistance of 370 Ω subtracted waterfall plot from V_G = 30 V to −30 V in 167 μV steps measured at T = 450 mK.

containing Ge. We attribute this layer as the channel through which the Ge atoms are transported into the Al pads.[13,14] The insets of Figure 1a show energy dispersive X-ray spectroscopy (EDX) chemical maps at the respective positions and prove an intact Si shell around the Ge NW segment and the Al NW. The monolithic heterostructure formation enables self-aligned quasi-1D c-Al leads contacting the Ge/Si segment. A SEM image of the actual heterostructure arrangement is shown in Figure 1b. For an analysis of the Al−Ge interface, high-resolution high-angle annular dark field (HAADF) scanning transmission electron microscopy (STEM) oriented along the [11$\bar{2}$] direction of observation of the Ge crystal was performed on a probe-corrected FEI Titan Themis working at 200 kV (obtained at the cyan dashed square shown in Figure 1b). All investigated Al−Ge interfaces showed a very sharp metal−semiconductor interface, and we observed an epitaxial relation between the exchanged c-Al and Ge part along the Ge(111) growth plane, without the visibility of any crystal defects. An intensity profile obtained in the HAADF STEM image (Figure 1c) shows that on going from the Ge segment to the converted c-Al region the intensity changes over about 1 nm. The lattice spacing was extracted using an averaged intensity profile over the interface and measuring the distances between the least intensity on each side of a column. However, if we measure the local lattice spacing, as shown in the inset, we find the last plane of higher HAADF STEM intensity has the lattice spacing close to the value of a Ge(111) plane (about 0.32 nm). The final Ge(111) plane is directly followed by a lower intensity plane with the lattice spacing close to the value expected for an Al(111) plane (0.24 nm), indicating a perfectly abrupt interface over the full diameter with no bending up to the atomic level. However, we have often observed that the Ge region extends at the NW surface into the converted Al region, only over a few nm and at a localized place (see Supporting Figure S1). Using this Al metallization scheme and consecutive annealing steps, the Ge/Si channel length can be tuned by the Al−Ge exchange procedure beyond lithographic limitations down to 10 nm (see Supporting Figure S2).

To investigate the electrical transport properties, the intrinsic Ge/Si core/shell NWs were integrated in back-gated FETs. A schematic illustration of the device architecture and the respective biasing is displayed in the upper inset of Figure 2a. The transport measurements were carried out using a two-probe configuration; hereafter we have subtracted the wiring resistance. The main plot of Figure 2b shows the comparison of room-temperature I/V characteristics at gate voltage (V_G = 0 V) of an intrinsic Ge NW (blue) and a Ge/Si core/shell NW (black) both with a physical transistor channel length of 2 μm. For the core/shell NW a clean confinement potential in the Ge core is expected[8,22] in view of the epitaxial growth of the Si shell resulting in a high mobility 1D hole gas[4,23] (see lower inset of Figure 2b). The origin of the hole gas is associated with the abrupt discontinuity of the band structure at the Ge−Si interface, showing a band offset of approximately 500 meV.[4] This causes holes to flow from Si to Ge to maintain a constant chemical potential throughout the arrangement. Consequently, the band edges are bent at the interface and holes are confined in the Ge close to the Ge−Si interface, forming a hole gas.[22] Thus, in comparison with the intrinsic Ge NW the resistance of the Ge/Si core/shell NW is more than 2 orders of magnitude lower. The first annealing cycle reduces the channel length of the Al−Ge/Si−Al NW heterostructures from 2 μm (black) to $L_{Ge/Si}$ = 470 nm (green). We observed a moderate decrease in resistance of about 60%, which we ascribe to a combined effect of the reduction of the channel length and a change of the contact architecture from the Al pad atop the Ge core to a quasi 1D monolithic Al−Ge contact. The second annealing cycle reduces the channel length further to $L_{Ge/Si}$ = 40 nm (red), resulting in a roughly 10-fold reduction in resistance (see upper inset). In comparison with a ballistic bare Ge NW based device of the same channel length, the resistance of the Ge/Si core/shell heterostructure is by a factor of 5 lower.[24] Therefore, even though multiple consecutive annealing cycles were performed, Ge/Si core/shell NWs still reveal a 1D hole characteristic, proving the thermal stability of the Si shell and the selective exchange of the Ge core. A log−log

DOI: 10.1021/acsnano.9b06809
ACS Nano 2019, 13, 14145−14151

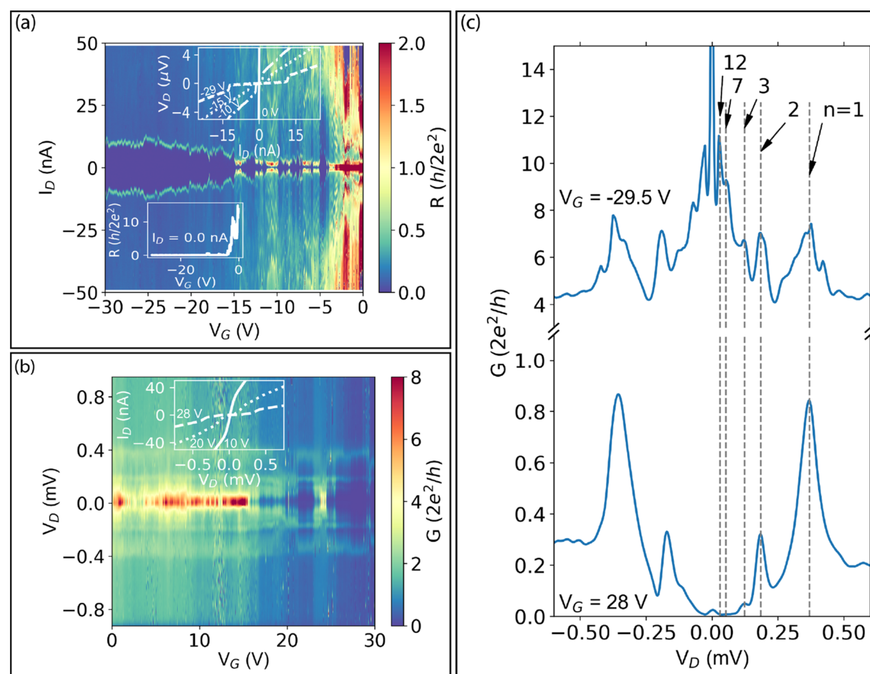

Figure 4. (a) Differential resistance dV_D/dI_D, with a wiring resistance of 370 Ω subtracted, plotted in units of the quantum resistance *versus* I_D and V_G. I_D was swept from negative to positive and V_G from 0 V to −30 V measured at 420 mK. The dark blue regions correspond to zero resistance and indicate superconductivity induced into the Ge/Si core/shell channel. The upper inset shows V_D *versus* I_D for four different V_G (0, −10, −15, −29 V). The lower inset shows a slice of differential resistance dV_D/dI_D at I_D = 0 nA with respect to V_G. (b) Differential conductance dI_D/dV_D, with a wiring resistance of 370 Ω subtracted, plotted in units of quantum resistance *versus* V_D and V_G. V_D was swept from negative to positive. The inset shows I_D *versus* V_D for three different V_G (10, 20, 28 V) (c) Differential conductance slice (dI_D/dV_D) with respect to V_D for V_G = −29.5 and 28 V measured at 450 mK.

representation of the I/V data shown in Figure 2b is supplied in Supporting Information Figure S3.

Figure 3a shows the conductance *vs* gate voltage (G−V_G) characteristic of the back-gated Ge/Si core/shell NW FET device with the channel length of $L_{Ge/Si}$ = 40 nm measured in the temperature range from T = 5 to 300 K. When the gate voltage is swept from positive to negative, the conductance increases; thus the device behaves like a p-type accumulation FET device.[25] Although charging and hysteresis effects should be significantly suppressed by passivating a Ge NW with a Si shell,[26] we note that a dependence on the V_G sweep direction for our Ge/Si core/shell NW heterostructure devices was found. Cooling the sample does not change the overall conductance, but at T = 150 K and even more pronounced for lower temperatures, distinctive plateau-like features can be observed. As the channel length of this particular device is below the scattering mean free path in Ge/Si core/shell NWs of 70 nm,[26] we associate this quantization of conductance in steps of $G_0 = 2e^2/h$ with one-dimensional spin-degenerate sub-band-resolved quantum ballistic transport.[4,27,28] Given that the Ge/Si core/shell segment is in the ballistic limit and that we are in a linear regime, we can estimate the transparency of the interface by linearly fitting $R = (R_0 + R_I)/n$,[29] blue curve of the inset, where $R_0 = h/2e^2$ is the quantized resistance and $R_I = R_0(1 - T)/T$ is the interface resistance due to scattering. In the inset the resistance ($R = 1/G$) of the plateaus taken at the points marked by black arrows are plotted against the inverse of the conducting channel number, associated with that plateau ($1/n$). The slope of the linear fit gives a value of $1.04R_0$, resulting in a transparency of approximately 96%. Furthermore, the G−V_G measurement recorded at T = 5 K hints at the conductance anomaly at $0.7G_0$ (blue arrow), which is considered as an intrinsic low-temperature sub-G_0 feature of mesoscopic devices.[30]

To investigate the observed plateaus below the superconducting transition temperature of the Al contacts (T_C = 1.19 K),[31] measurements were carried out in a pumped ^{3}He cryostat. Figure 3b shows traces of the bias voltage dependent differential conductance ($G = I_D/V_D$) for fixed gate voltages ranging from V_G = 30 V to −30 V with a step size of 167 μV at T = 450 mK. The conductance traces bunch into five thick lines of constant conductance, separated by regions of low trace density. Five conductance channels are clearly visible in Figure 3b, with each bunching region occurring near an integer multiple of G_0. Impressively, these low-temperature measurements, which were performed two and a half years after, still present the quantized levels with only a slightly lower transparency (see Supporting Figure S4).

Considering the low temperature of the measurement ($T < T_C$), the conductance peak at zero bias is a clear first indication of induced superconductivity in the Ge/Si core/shell segment. Further, an indication of quantization of these superconducting features is supplied by Supporting Figure S5, which shows an overlay of the differential conductance recorded above (T = 2 K) and below (T = 450 mK) T_C. The observation of quantized conductance further endorses our achievement of a near atomically precise interface between Al contacts and Ge/Si core/shell segments.

To investigate the high conductance regime for gate voltages in the range −30 V < V_G < 0 V, we carried out current biasing measurements at T = 420 mK. For this measurement, the gate voltage was swept from 0 V to −30 V. For each gate voltage the voltage was recorded for sweeping the current from −50 nA to 50 nA. Figure 4a shows the differential resistance (dV_D/

DOI: 10.1021/acsnano.9b06809
ACS Nano 2019, 13, 14145−14151

dI_D) as a function of bias current and gate voltage in the range -30 V < V_G < 0 V. The density plot clearly shows an extended region of near-zero resistance centered around I_D = 0 nA and V_G < -5 V, suggesting there is a dissipationless supercurrent regime through the Ge/Si core/shell segment. To illustrate the V_G dependence on the transport dynamics, the lower inset shows a resistance slice at I_D = 0 nA. Between V_G = 0 V and -3 V a regime of high zero-bias resistance, on the order of several quantum of resistance, is observed. This regime is followed by a strongly decreasing resistance of the device as the gate voltage is decreased. Decreasing from V_G = -3 V, the zero-bias resistance of the heterostructure device drops abruptly and finally converges to a small finite resistance of 25 Ω. We attribute this finite resistance to thermally activated phase slips. Such phase slips are of significance in Josephson junctions, when the Josephson energy (estimated here at $E_J = \Phi_0 I_C/2\Pi \approx 5 \times 10^{-24}$ J) is on the order of the thermal energy ($k_B T \approx 6 \times 10^{-24}$ J).[32]

To further show the dependence of I_C on the gate voltage induced electric field, the upper inset of Figure 4a shows the I/V characteristic of the heterostructure device for particular gate voltages, illustrating the ability to tune I_C. These observations clearly demonstrate that such a device, with a short channel, possesses a gate voltage mediated superconducting proximity effect.[33,34] As the Ge/Si core/shell heterostructure device shows characteristics of a p-type semiconductor, a more negative V_G increases the number of conductance channels, resulting in higher I_C and an increased conductance in the normal state. At approximately V_G = -25 V, the critical current saturates at a value of about I_C = 15 nA.

Figure 4b shows the respective plot in the gate-voltage range between V_G = 0 and 30 V based on a measurement of differential conductance (dI_D/dV_D) as a function of bias voltage and gate voltage. The inset shows raw I/V curves for V_G = 28, 20, and 10 V, further illustrating the transport dynamics of the device. The density plot reveals that even for a high positive gate voltage, up to V_G = 30 V, there are no Coulomb blockade effects, indicating the absence of a quantum dot regime. This is supported by the significant conductivity outside the superconducting gap of V_G = 28 V of approximately $0.3G_0$. This observation is in contrast to pure Si- or Ge-based devices featuring Schottky barriers[20] or Ge/Si core/shell-based NW devices contacting the Si shell,[35] forming a tunnel barrier at low temperatures. These findings further indicate that our Al–Ge/Si–Al heterostructure devices feature highly transparent contacts to the 1D hole gas, which is in good agreement with Xiang *et al.*[8] In the low conducting regime (25 V < V_G < 30 V) we observe a superconducting gap with a minimum gap ratio of $\langle G_G\rangle/\langle G_N\rangle$ = 0.03, where $\langle G_G\rangle$ is the average conductance inside the gap, across a V_D range from -0.05 to 0.05 mV, and $\langle G_N\rangle$ is the average conductance outside the gap, across a V_D range from -0.7 to -0.6 mV.

Figure 4c shows a slice of the differential conductance with respect to V_D in the low conducting regime (V_G = 28 V, taken from Figure 4b) and the high conducting regime (V_G = -29.5 V, taken from Supporting Figure S6) at T = 420 mK. In both regimes, a family of peaks are observed symmetrically around V_D = 0 V. In the high conducting regime, the peak at zero bias shows a differential conductance higher than $200G_0$ and corresponds to the "infinite conductivity" of the superconducting state of the Ge/Si core/shell channel. Further, the peaks at finite V_D correspond to the subharmonic energy-gap structure caused by multiple Andreev reflections (MARs),[18] with peak positions given by $eV_n = 2\Delta/n$.[34] Such features arise from a progressive increase of the incident carrier energy as the carrier reflects between the two interfaces and thus mark Andreev channels present in superconductor–normal–superconductor (S–N–S) junctions for applying bias voltages below the superconducting gap. Taking the superconducting gap (Δ) to be half of, V_D = 0.37 mV, the position of the first conductance peak (n = 1), we obtain 0.185 meV and we observe five MARs of n = 1, 2, 3, 7, and 12 (see dashed lines in Figure 4c). Interestingly, we observe a conductance peak at 0.44 mV that would indicate a slightly larger superconducting gap. However, as all other peaks do not match to this gap, we believe that this feature could be associated with the slightly higher T_C of the polycrystalline Al contact pads. The first three Andreev peaks of the V_G = -29.5 V slice align perfectly with the observed peaks at V_G = 28 V. The stability of the MARs through 60 V of gate tuning (see Supporting Figure S7) further endorses the exceptional interface quality that we have achieved.

By fitting I/V characteristic curves above the Al superconducting gap ($V_D > 2\Delta/e$) (see Supporting Figure S8) we calculated the normal resistance (R_n) and the excess current (I_{exc}) for V_G < 0 V. R_n converges at V_G = -25 V to 2.98 kΩ. Using the BTK[36] model we retrieve a barrier strength of Z = 0.1, resulting in a transparency of 99%, which is consistent with the transparency calculated from the quantized conductance plateaus.

CONCLUSION

In conclusion, we report the synthesis and electrical characterization of crystalline axial Al–Ge/Si–Al core/shell NW heterostructures. We have devised and implemented an annealing scheme to fabricate ultrascaled Al–Ge/Si–Al heterostructures with highly transparent contacts. Through consecutive annealing cycles, the length of the Ge segment can be tuned beyond lithographic limitations. High-resolution HAADF STEM and EDX measurements show an abrupt atomically precise interface between the c-Al leads and Ge with an intact Si shell around the entire Al–Ge–Al heterostructure. The integration of these 1D hole gas NW heterostructures in back-gated FETs enabled the investigation of their transport properties. Observations of stable MARs and quantized conductance affirmed the great quality of the interface and a high contact transparency, greater than 96% of the metal–semiconductor contact. The observation of a supercurrent up to 15 nA at 420 mK and its ability to be tuned by a gate make these devices suitable candidates for gatemon qubits. Further, the promising gap ratio of $\langle G_G\rangle/\langle G_N\rangle$ = 0.03 in the low-conductance regime is promising for the observation of Majorana zero modes. The opportunity to tune the electrical properties of these single-crystalline metal–semiconductor heterostructures provides a promising platform toward practical applications of future ultrascaled axial and radial nanoelectronic devices.

METHODS AND EXPERIMENTAL

Device Fabrication. The starting materials are vapor–liquid–solid-grown core/shell NWs with a Ge NW core diameter of 30 nm and a Si shell thickness of about 3 nm covered by a thin layer of native oxide.[8,4] The NWs were drop casted onto an oxidized highly p-doped Si substrate, and the Ge core NW was contacted by Al pads fabricated by electron beam lithography, 100 nm Al sputter deposition, and lift-off techniques. To gain access to the Ge core NW, the Si shell was

DOI: 10.1021/acsnano.9b06809
ACS Nano 2019, 13, 14145–14151

selectively removed by wet chemical etching for 10 s in buffered HF (7:1) to remove the native oxide layer followed by a 15 s treatment in KOH (30%). The Al−Ge exchange reaction is induced by rapid thermal annealing at a temperature of T = 674 K in a forming gas atmosphere and results in the substitution of the Ge core by c-Al.[12] The diameter of the Al core and the thickness of the Si shell are thereby inherited from the initial Ge/Si core/shell NW geometry. Facilitating the proposed heterostructure formation scheme[13] allows the integration of the core/shell heterostructures with tunable channel lengths in a FET architecture, with the highly p-doped substrate acting as back-gate.

Electrical Characterization. The electrical measurements at room temperature and ambient conditions were performed using a combination of a semiconductor analyzer (HP 4156B) and a probe station. To minimize the influence of ambient light as well as electromagnetic fields, the probe station is placed in a dark box. Low-temperature measurements (5−298 K) were performed in a vacuum at a background pressure of approximately 2.5×10^{-5} mbar using a ^{4}He cryostat (Cryo Industries CRC-102) and a semiconductor analyzer (Keysight B1500A). Electrical measurements below T = 5 K were carried out using a self-built pumped ^{3}He cryostat with a base temperature of T = 400 mK. Noise filtering was achieved using a room-temperature Pi-filter and at low temperature thermal coax of approximately 1 m in length. The resistance of the fridge wiring was independently measured to be 370 Ω at 420 mK. The device was probed at low temperature using both voltage and current biasing techniques with a National Instruments PCI DAC/ADC high-frequency card. In the voltage biasing scheme a voltage divider consisting of 50 kΩ/50 Ω was used to reduce the amplitude of the voltage source. A Femto variable gain transimpedance amplifier (DCPCA-200) was used to convert and amplify the induced current to a voltage signal measured by the NI card. In the current biasing scheme a 10 MΩ resistor was used to convert the voltage signal to a current signal with a maximum amplitude of 1 μA. The current was applied to the sample, which was grounded at one end. The potential difference across the sample was amplified by two NF Electronic Instruments low-noise preamplifiers (LI-75A), each of a gain of 100, in series. The back gate was biased using a Yokogawa programmable voltage source.

ASSOCIATED CONTENT

Supporting Information

The Supporting Information is available free of charge at https://pubs.acs.org/doi/10.1021/acsnano.9b06809.

STEM images of the same NW viewed under different angles, compilation of SEM images showing Al−Ge/Si−Al core/shell NW heterostructures with different channel lengths, log−log version of the I/V data presented in Figure 2, additional $G-V_G$ measurements at T = 450 mK and 5 K, overlay of bias spectroscopy measurements at T = 450 K and 2 K, additional maps of the differential resistance and conductance, V/I curve measured at T = 420 mK to show the fitting procedure (PDF)

AUTHOR INFORMATION

Corresponding Author

*E-mail: olivier.buisson@neel.cnrs.fr.

ORCID

Masiar Sistani: 0000-0001-5730-234X
Roman B. G. Kramer: 0000-0001-8598-4720
Minh Anh Luong: 0000-0002-0876-2400
Martien I. den Hertog: 0000-0003-0781-9249
Jun Yao: 0000-0002-5269-3190
Charles M. Lieber: 0000-0002-6660-2456
Alois Lugstein: 0000-0001-5693-4775

Author Contributions

¶M. Sistani and J. Delaforce contributed equally.

Author Contributions

M.S. performed the device fabrication and experimental design. M.S., J.D., C.N., and R.K. conducted the electrical characterization. A.L., O.B., C.N., and J.S. conceived the project, contributed essentially to the experimental design, and provided expertise on theoretical interpretations. M.I.H., L.M.A., and E.R. carried out the TEM and EDX measurements and analysis. J.Y. and C.M.L. provided the Ge/Si core/shell NWs and helpful feedback and commented on the manuscript. All authors analyzed the results and helped shape the research and manuscript.

Notes

The authors declare no competing financial interest.

ACKNOWLEDGMENTS

The authors gratefully acknowledge financial support by the Austrian Science Fund (FWF): project no. P29729-N27. The authors further thank the Center for Micro- and Nanostructures for providing the cleanroom facilities. We acknowledge support from the Laboratoire d'Excellence LANEF in Grenoble (ANR-10-LABX-51-01). Financial support from the ANR-COSMOS (ANR-12-JS10-0002) project and the ANR-QPS nanowires (ANR-15-CE30-0021) project is acknowledged. We acknowledge support from Campus France in the framework of PHC AMADEUS 2016 for PROJET No. 35592PB. J.D. acknowledges the European Union's Horizon 2020 research and innovation program under the Marie Skłodowska-Curie grant agreement no. 754303. This project has also received funding from the European Research Council under the European Union's H2020 Research and Innovation program *via* the e-See project (grant #758385). We benefitted from the access to the Nano characterization platform (PFNC) in CEA Minatec Grenoble. The authors would like to acknowledge S. De Franceschi, F. Lefloch, K. Rafsanjani, and T. Vethaak for beneficial discussions.

REFERENCES

(1) Zhao, X.; Wei, C. M.; Yang, L.; Chou, M. Y. Quantum Confinement and Electronic Properties of Silicon Nanowires. *Phys. Rev. Lett.* **2004**, *92*, 236805.
(2) Lin, L.; Li, Z.; Feng, J.; Zhang, Z. Indirect to Direct Band Gap Transition in Ultra-Thin Silicon Films. *Phys. Chem. Chem. Phys.* **2013**, *15*, 6063.
(3) Irrera, A.; Artoni, P.; Iacona, F.; Pecora, E. F.; Franzò, G.; Galli, M.; Fazio, B.; Boninelli, S.; Priolo, F. Quantum Confinement and Electroluminescence in Ultrathin Silicon Nanowires Fabricated by a Maskless Etching Technique. *Nanotechnology* **2012**, *23*, No. 075204.
(4) Lu, W.; Xiang, J.; Timko, B. P.; Wu, Y.; Lieber, C. M. One-Dimensional Hole Gas in Germanium/Silicon Nanowire Heterostructures. *Proc. Natl. Acad. Sci. U. S. A.* **2005**, *102*, 10046−10051.
(5) Ray, S. K.; Katiyar, A. K.; Raychaudhuri, A. K. One-Dimensional Si/Ge Nanowires and Their Heterostructures for Multifunctional Applications - A Review. *Nanotechnology* **2017**, *28*, No. 092001.
(6) Xiang, J.; Lu, W.; Hu, Y.; Wu, Y.; Yan, H.; Lieber, C. M. Ge/Si Nanowire Heterostructures as High-Performance Field-Effect Transistors. *Nature* **2006**, *441*, 489−493.
(7) Hu, Y.; Xiang, J.; Liang, G.; Yan, H.; Lieber, C. M. Sub-100 Nanometer Channel Length Ge/Si Nanowire Transistors with Potential for 2 THz Switching Speed. *Nano Lett.* **2008**, *8*, 925−930.

(8) Xiang, J.; Vidan, A.; Tinkham, M.; Westervelt, R. M.; Lieber, C. M. Ge/Si Nanowire Mesoscopic Josephson Junctions. *Nat. Nanotechnol.* **2006**, *1*, 208−213.
(9) Conesa-Boj, S.; Li, A.; Koelling, S.; Brauns, M.; Ridderbos, J.; Nguyen, T. T.; Verheijen, M. A.; Koenraad, P. M.; Zwanenburg, F. A.; Bakkers, E. P. A. M. Boosting Hole Mobility in Coherently Strained [110]-Oriented Ge−Si Core−Shell Nanowires. *Nano Lett.* **2017**, *17*, 2259−2264.
(10) Hyun, J. K.; Zhang, S.; Lauhon, L. J. Nanowire Heterostructures. *Annu. Rev. Mater. Res.* **2013**, *43*, 451−479.
(11) Zheng, H.; Li, Y.; Liu, H.; Yin, X.; Li, Y. Construction of Heterostructure Materials Toward Functionality. *Chem. Soc. Rev.* **2011**, *40*, 4506.
(12) Kral, S.; Zeiner, C.; Stöger-Pollach, M.; Bertagnolli, E.; den Hertog, M. I.; Lopez-Haro, M.; Robin, E.; El Hajraoui, K.; Lugstein, A. Abrupt Schottky Junctions in Al/Ge Nanowire Heterostructures. *Nano Lett.* **2015**, *15*, 4783−7.
(13) Sistani, M.; Luong, M. A.; den Hertog, M. I.; Robin, E.; Spies, M.; Fernandez, B.; Yao, J.; Bertagnolli, E.; Lugstein, A. Monolithic Axial and Radial Metal−Semiconductor Nanowire Heterostructures. *Nano Lett.* **2018**, *18*, 7692−7697.
(14) El hajraoui, K.; Luong, M. A.; Robin, E.; Brunbauer, F.; Zeiner, C.; Lugstein, A.; Gentile, P.; Rouvière, J.-L.; Den Hertog, M. *In Situ* Transmission Electron Microscopy Analysis of Aluminum−Germanium Nanowire Solid-State Reaction. *Nano Lett.* **2019**, *19*, 2897−2904.
(15) Ridderbos, J.; Brauns, M.; Shen, J.; de Vries, F. K.; Li, A.; Bakkers, E. P. A. M.; Brinkman, A.; Zwanenburg, F. A. Josephson Effect in a Few-Hole Quantum Dot. *Adv. Mater.* **2018**, *30*, 1802257.
(16) Vigneau, F.; Mizokuchi, R.; Zanuz, D. C.; Huang, X.; Tan, S.; Maurand, R.; Frolov, S.; Sammak, A.; Scappucci, G.; Lefloch, F.; De Franceschi, S. Germanium Quantum-Well Josephson Field-Effect Transistors and Interferometers. *Nano Lett.* **2019**, *19*, 1023−1027.
(17) Ridderbos, J.; Brauns, M.; Li, A.; Bakkers, E. P. A. M.; Brinkman, A.; van der Wiel, W. G.; Zwanenburg, F. A. Multiple Andreev Reflections and Shapiro Steps in a Ge-Si Nanowire Josephson Junction. *Phys. Rev. Mater.* **2019**, *3*, No. 084803.
(18) Ihn, T. *Electronic Quantum Transport in Mesoscopic Semiconductor Structures*; Springer Tracts in Modern Physics; Springer: New York, 2004.
(19) Larsen, T. W.; Petersson, K. D.; Kuemmeth, F.; Jespersen, T. S.; Krogstrup, P.; Nygård, J.; Marcus, C. M. Semiconductor-Nanowire-Based Superconducting Qubit. *Phys. Rev. Lett.* **2015**, *115*, 127001.
(20) Zwanenburg, F. A.; Van Loon, A. A.; Steele, G. A.; Van Rijmenam, C. E. W. M.; Balder, T.; Fang, Y.; Lieber, C. M.; Kouwenhoven, L. P. Ultrasmall Silicon Quantum Dots. *J. Appl. Phys.* **2009**, *105*, 124314.
(21) Wagner, R. S.; Ellis, W. C. Vapor-Liquid-Solid Mechanism of Single Crystal Growth. *Appl. Phys. Lett.* **1964**, *4*, 89−90.
(22) Fukata, N.; Yu, M.; Jevasuwan, W.; Takei, T.; Bando, Y.; Wu, W.; Wang, Z. L. Clear Experimental Demonstration of Hole Gas Accumulation in Ge/Si Core−Shell Nanowires. *ACS Nano* **2015**, *9*, 12182−12188.
(23) Sze, S. M.; Ng, K. K. *Physics of Semiconductor Devices*; John Wiley & Sons, Inc.: Hoboken, NJ, 2006.
(24) Sistani, M.; Staudinger, P.; Greil, J.; Holzbauer, M.; Detz, H.; Bertagnolli, E.; Lugstein, A. Room-Temperature Quantum Ballistic Transport in Monolithic Ultrascaled Al−Ge−Al Nanowire Heterostructures. *Nano Lett.* **2017**, *17*, 4556−4561.
(25) Greytak, A. B.; Lauhon, L. J.; Gudiksen, M. S.; Lieber, C. M. Growth and Transport Properties of Complementary Germanium Nanowire Field-Effect Transistors. *Appl. Phys. Lett.* **2004**, *84*, 4176−4178.
(26) Kotekar-Patil, D.; Nguyen, B.-M.; Yoo, J.; Dayeh, S. A.; Frolov, S. M. Quasiballistic Quantum Transport Through Ge/Si Core/Shell Nanowires. *Nanotechnology* **2017**, *28*, 385204.
(27) Beenakker, C. W. J.; van Houten, H. *Quantum Transport in Semiconductor Nanostructures*; Elsevier Academic Press: Amsterdam, 1991.
(28) Kubis, T. C. *Quantum Transport in Semiconductor Nanostructures*, Selected Topics of Semiconductor Physics and Technology; Walter Schottky Institut, Technische Universität München, 2009.
(29) Datta, S. *Electronic Transport in Mesoscopic Systems*; Cambridge University Press: Cambridge, 1995.
(30) Micolich, A. P. What Lurks Below the Last Plateau: Experimental Studies of the $0.7 \times 2e^2/h$ Conductance Anomaly in One-Dimensional Systems. *J. Phys.: Condens. Matter* **2011**, *23*, 443201.
(31) Matsuo, S.; Sugiura, H.; Noguchi, S. Superconducting Transition Temperature of Aluminum, Indium, and Lead Fine Particles. *J. Low Temp. Phys.* **1974**, *15*, 481−490.
(32) Tinkham, M. *Introduction to Superconductivity*; Dover Publications, Inc.: New York, 2004.
(33) Buckel, W.; Kleiner, R. *Superconductivity: Fundamentals and Applications, A Text Book*; Wiley-VCH Verlag GmbH: Weinheim, 2004.
(34) Schäpers, T. *Superconductor/Semiconductor Junctions*; Springer Tracts in Modern Physics; Springer: Berlin Heidelberg, 2001.
(35) Kloeffel, C.; Trif, M.; Loss, D. Strong Spin-Orbit Interaction and Helical Hole States in Ge/Si Nanowires. *Phys. Rev. B: Condens. Matter Mater. Phys.* **2011**, *84*, 195314.
(36) Blonder, G. E.; Tinkham, M.; Klapwijk, T. M. Transition From Metallic to Tunneling Regimes in Superconducting Microconstrictions: Excess Current, Charge Imbalance, and Supercurrent Conversion. *Phys. Rev. B: Condens. Matter Mater. Phys.* **1982**, *25*, 4515−4532.

DOI: 10.1021/acsnano.9b06809
ACS Nano 2019, 13, 14145−14151